processes

MDPI

Article

Research on Overburden Movement and Surface Subsidence Control of Partial Backfill Mining in Deep Coal Seams Based on NPR-DDA

Chao Wang [1], Cheng Hu [2], Weiming Gao [1], Yingshi Gu [3] and Quan Zhang [2,*]

[1] Yankuang Energy Group Co., Ltd., Jining 273500, China
[2] Faculty of Engineering, China University of Geosciences, Wuhan 430074, China
[3] Inner Mongolia Haosheng Coal Industry Co., Ltd., Ordos 017000, China
* Correspondence: quanzhang@cug.edu.cn

Abstract

Targeting the problem of surface subsidence caused by deep coal seam mining, using the 1210 panel of the Shilawusu Coal Mine as the background and based on field-measured surface subsidence data, a numerical model of mining-induced overburden behavior under partial backfill mining in deep coal seams was constructed using the NPR-DDA bonded particle model. The evolutionary laws of overburden fracture and movement during the working face advancement were systematically studied; the dynamic characteristics of the vertical displacement and stress fields were revealed; and the effects of the backfill rate, backfill working face width, caving working face width, and section coal pillar width on surface subsidence were investigated through one-factor-at-a-time analyses to identify the response trends under the specified simulation conditions. The results show that: the measured surface subsidence exhibits an asymmetric, funnel-shaped progressive evolution, with the maximum subsidence (187 mm) located at monitoring point H52 and shifted toward the left side of the goaf; when advanced to 100 m, the immediate roof collapses first (maximum subsidence of 4.4 m), and when advanced to 300 m, sub-key stratum 1 collapses entirely while the bed-separation space beneath sub-key stratum 2 shrinks, resulting in compression and consolidation of the broken rock mass in the goaf; and partial backfilling plays an active supporting role, with the average vertical stress in the central backfilling zone reaching 19.38 MPa; under the conditions of the respective simulation groups, increasing the backfill rate, backfill working face width, and section coal pillar width reduces the magnitude of maximum surface subsidence from 1501 to 652 mm, from 1632 to 930 mm, and from 1264 to 513 mm, respectively, whereas increasing the caving working face width increases it from 1023 to 2357 mm. The findings provide a reference for evaluating partial backfill mining schemes for the unmined 1210 panel at the Shilawusu Coal Mine.

Keywords: deep coal mining; partial backfill mining; NPR-DDA numerical simulation; overburden fracture evolution; surface subsidence

Check for updates

Academic Editor: Evangelos Tsotsas

Received: 27 September 2026
Revised: 26 October 2026
Accepted: 26 October 2026
Published: 31 October 2026

Copyright: © 2026 by the authors. Licensee MDPI, Basel, Switzerland. This article is an open access article distributed under the terms and conditions of the Creative Commons Attribution (CC BY) license.

1. Introduction

With the gradual depletion of shallow coal resources in China, coal mining has comprehensively transitioned into the deep-mining stage. Currently, China ranks first globally in the number of deep mines with an average mining depth exceeding 700 m. Deep mining is confronted with a complex environment characterized by three highs and one disturbance, leading to significantly more intense mining responses compared to shallow operations. The

 https://doi.org/10.3390/pr14213496

resulting surface subsidence has emerged as a critical challenge that degrades the ecology of mining areas and threatens the safety of buildings, structures, and major engineering projects. It not only directly causes the destruction of arable land and structural cracking but also has the potential to trigger secondary geological disasters such as landslides and debris flows. According to statistics, the area of surface subsidence caused by coal mining in China has reached 6000 km^2, and it is increasing at a rate of 240 km^2 per year [1]; Meanwhile, the national volume of coal trapped under buildings, railways, and water bodies (commonly known as "three-under" coal) has reached 25 billion tons, which is primarily concentrated in the densely populated East China region [2]. How to effectively control surface subsidence while ensuring the resource recovery rate is a core scientific problem that urgently needs to be solved for the green and safe mining of deep coal.

Currently, surface subsidence control technologies are primarily divided into subsidence reduction technologies based on partial mining (such as strip mining and room-and-pillar mining) and subsidence reduction technologies based on backfill support (such as full backfill mining, overburden bed-separation grouting, etc.) [3,4]. Strip mining controls subsidence by retaining coal pillars for support, and its core lies in controlling the mining width within the critical mining width [5], but the hidden danger of long-term instability of the residual coal pillars limits its application. In contrast, backfill mining achieves active roof support by backfilling the goaf, which overcomes the hidden danger of long-term instability of coal pillars and can maintain the long-term balance of the overburden structure [6–10]. Yang et al. constructed a multi-horizon synergistic control technology system for thick coal seam mining [11]; Ma established an elastic foundation beam and limit equilibrium mechanical model [12]; Zhang established a strata control model for the pre-mining, trial-mining, and backfilling stages, and derived analytical expressions for load, caving step distance, and subsidence amount [13]; Li et al. proposed the concept of limit advancing speed in backfill mining [14]; Zhou established an overburden deformation mechanical model from the perspectives of beams and plates respectively, focusing on analyzing the deformation characteristics of the roof [15].

From the perspective of layout, backfill mining is divided into full backfilling and partial backfilling. The core of partial backfilling lies in the "backfill + coal pillar" composite support, that is, backfilling in partial areas of the goaf, while retaining coal pillars or adopting the caving method for management in the remaining areas, with the backfill body and coal pillars jointly bearing the overburden load [16]. Compared with full backfilling, partial backfilling can significantly reduce material consumption and costs; compared with simple strip mining, the introduction of the backfill body can substantially improve the recovery rate. Strip backfill mining, as a typical representative, achieves the unification of safety and efficiency by first conducting longwall backfilling and then recovering the coal pillars after the backfill reaches its strength. For example, Guo et al. proposed an L-shaped paste backfill technology to precisely support the roof [16]; Hao et al. utilized construction waste backfilling to achieve the safe recovery of coal pillars, with a maximum surface subsidence of only 44 mm [17]; Zhu et al. proposed a design method for subsidence control in strip backfilling, clarifying the influence of backfill parameters on the anti-deformation ability of buildings [18]; Wang et al. proposed a backfill strip mining method under thick unconsolidated layers, determining the reasonable working face dimensions and mining height, which reduced the maximum surface subsidence by 92% compared to longwall mining [19]; Du et al. proposed a new method of partial paste backfilling in fully mechanized caving faces and analyzed the influence of backfill structural factors on the subsidence reduction effect [20]; Liu et al. revealed through their research that the intermittent mining and backfilling method can effectively mitigate overburden damage and surface subsidence [21].

Taking the Shilawusu Coal Mine as the engineering background, this paper constructs a numerical model of mining-induced overburden behavior under partial backfill mining in deep coal seams, based on the bonded particle numerical model in NPR-DDA. It systematically reveals the characteristics of overburden fracture and movement, as well as the vertical displacement and stress fields under partial backfilling conditions, and quantitatively analyzes the influences of the backfill rate, backfill working-face width, caving working-face width, and section coal-pillar width on the surface subsidence control effect. The parametric investigation adopts a one-factor-at-a-time approach to identify the effects of individual factors on surface subsidence under the corresponding simulation conditions, providing a reference for evaluating partial backfill mining schemes and subsidence control measures for the 1210 panel at the Shilawusu Coal Mine.

2. Engineering Background

The Shilawusu Coal Mine is located in Ejin Horo Banner, Ordos City, Inner Mongolia, and belongs to the Nalin Caideng exploration block of the Dongsheng Coalfield. Provincial Highway S313 (Uxin Banner–Fugu) passes approximately 10 km north of the mine field, and it connects to National Highway G210 and the Baotou-Maoming Expressway 8 km to the east, providing convenient transportation. The 1210 panel is located in the middle of the south wing of the No. 12 panel area, adjacent to the 1208 panel to the west and bounded by the main roadway protection coal pillar to the north. The 1210 panel has a panel length of 290 m, an advancing length of 3240 m, and an area of 936,700 m^2. The coal seam floor elevation ranges from +682.3 to +698.2 m. The surface consists of sandy land, with surface elevations ranging from +1337.3 to +1366.5 m (averaging +1350.0 m). See Figure 1.

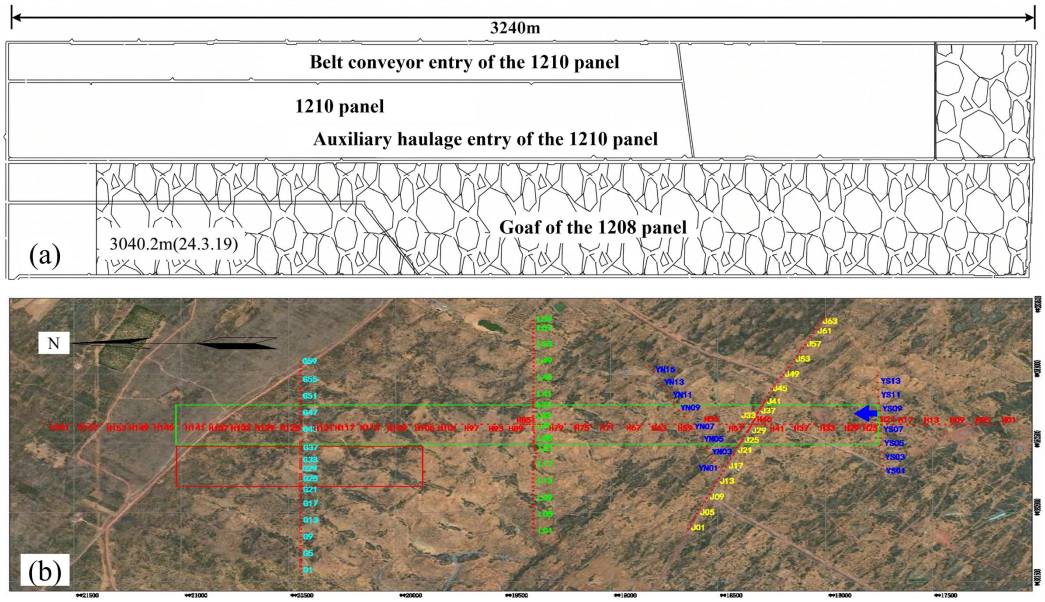


Figure 1. Layout of 1208 panel and 1210 panel in mining area. (**a**) Neighboring relationships of the 1210 panel; (**b**) Layout diagram of monitoring points for the 1208 panel.

In the southern section, the merged zone of the 2-2 upper and 2-2 middle coal seams is mined, with an average coal thickness of 8.8 m; in the northern section, the 2-2 upper coal seam is mined, with an average thickness of 5.3 m, exhibiting stable coal seam thickness. The working face floor elevation ranges from +690.7 to +700.3 m (averaging +693.0 m). Fully mechanized top-coal caving technology is adopted for mining, and the full caving method is utilized for roof management.

Based on the actual measurement data from the strike profile (93 monitoring points) and the dip profile (59 monitoring points) of the 1208 panel in the Shilawusu Coal Mine, the mining-induced surface subsidence deformation curves were plotted (Figure 2). The results indicate that the surface subsidence process exhibits significant asymmetry and progressive evolution characteristics, presenting an overall funnel-shaped distribution. Both the strike and dip profiles begin at the surface movement boundaries with near-zero subsidence (monitoring points H01 and L01); as they advance towards the center of the goaf, the slope of the subsidence curve continuously increases; after crossing the inflection points of half the maximum subsidence (H28–H75 for the strike profile, L17–L49 for the dip profile), the deformation rate and magnitude increase significantly. The maximum surface subsidence value (187 mm) is located at monitoring point H52, which is shifted to the left relative to the geometric center of the goaf.

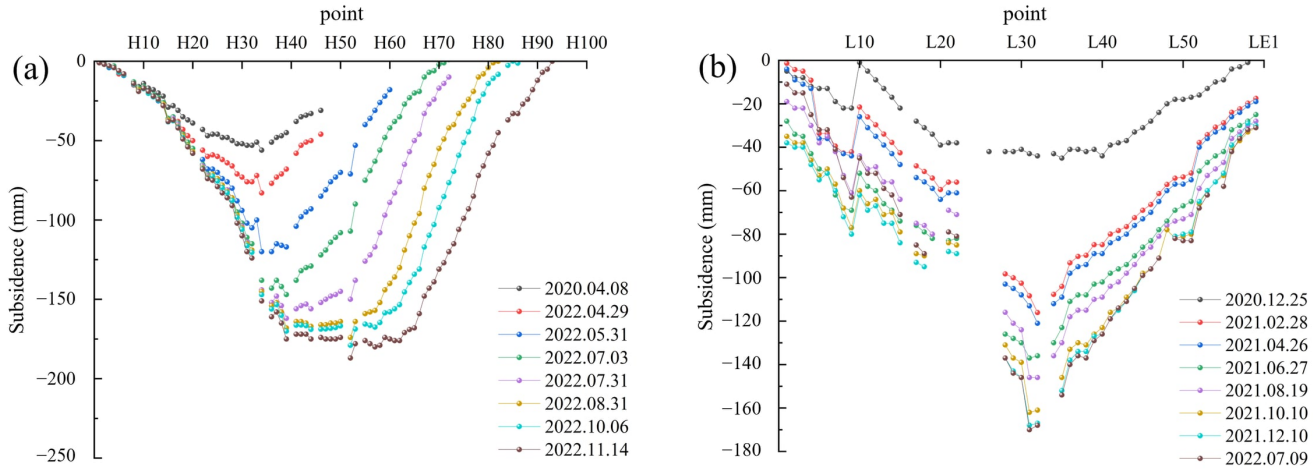


Figure 2. Surface subsidence curves of the 1208 panel in the Shilawusu Coal Mine. (**a**) Strike direction; (**b**) Dip direction.

3. NPR-DDA Numerical Analysis of Partial Backfill Mining in Deep Coal Seams

3.1. NPR-DDA Numerical Model

The historical surface subsidence measurements from the completed 1208 panel, presented in Section 2, are used to characterize mining-induced subsidence and establish the need for subsidence control in subsequent mining. The 1210 panel was unmined at the time of this study and provides the geological and engineering background for the numerical investigation. An NPR-DDA model of partial backfill mining is established to analyze overburden fracturing, movement, and stress distributions during simulated mining. The individual effects of backfill rate, backfill working face width, caving working face width, and section coal pillar width on surface subsidence are examined under the corresponding fixed conditions, providing a reference for evaluating mining schemes for the 1210 panel.

Based on Newtonian mechanics and the principle of minimum potential energy, the DDA method treats the research object as mutually independent, non-penetrating blocks and constructs a global equilibrium equation system, employing implicit iteration to solve for block displacements. As a kinematic analysis framework, this method is not only applicable to static research but can also be extended to the field of dynamics, excelling particularly in handling large displacements and nonlinear deformation problems of rock masses. In the DDA computational architecture, the bonded particle numerical model can be transformed into sub-matrices and superimposed onto the governing equations, reflecting the model's

impact on the disk system by solving for displacement unknowns. Huang [22] derived its sub-matrix expressions using the principle of minimum potential energy. As shown in Figure 3, assuming a rectangular bonded element (B_1, B_2, B_3, B_4) is applied between disk *i* and disk *j*, this element contains two normal springs and one tangential spring as load-bearing components. Specifically, the tangential spring restricts the relative tangential sliding between two contact points (P_1, P_2), while the normal springs restrict the relative normal displacements of four designated points (P_3, P_4, P_5, P_6).

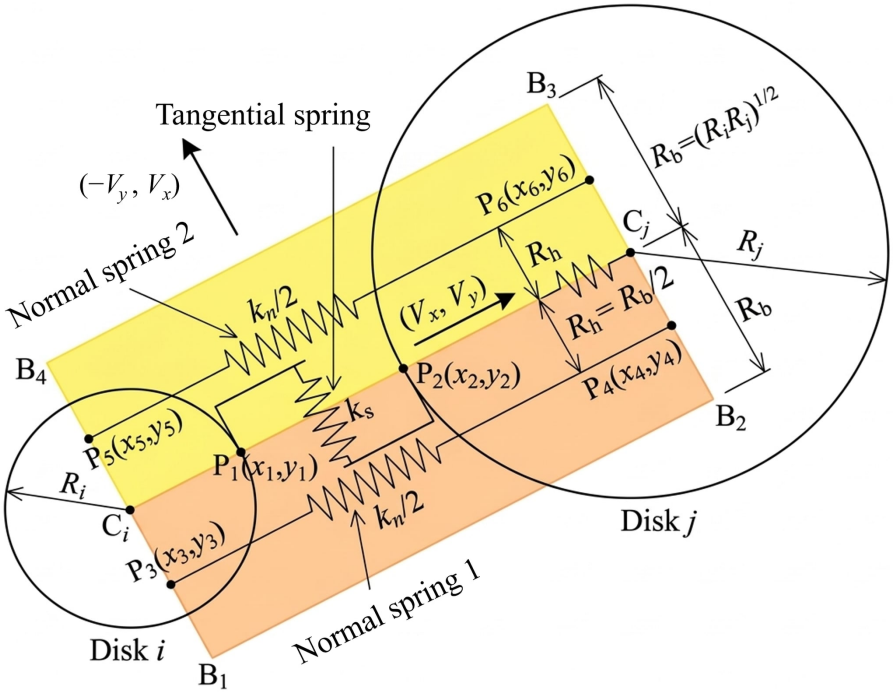


Figure 3. Schematic diagram of the bonded particle numerical model.

Twenty-three representative rock specimens were selected for uniaxial compression testing. The specimens were loaded under displacement control at a constant rate of 0.01 mm/s until failure. The testing apparatus is shown in Figure 4. A numerical model of uniaxial compression was then constructed, and the microscopic parameters were determined through trial and error. A representative calibration result is presented in Figure 5, showing good agreement between the numerical and experimental results.

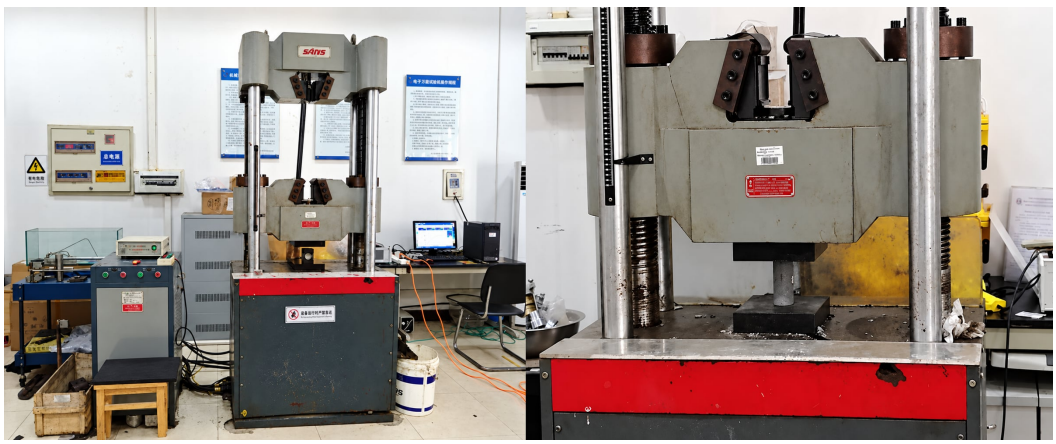


Figure 4. Apparatus for uniaxial compression testing.

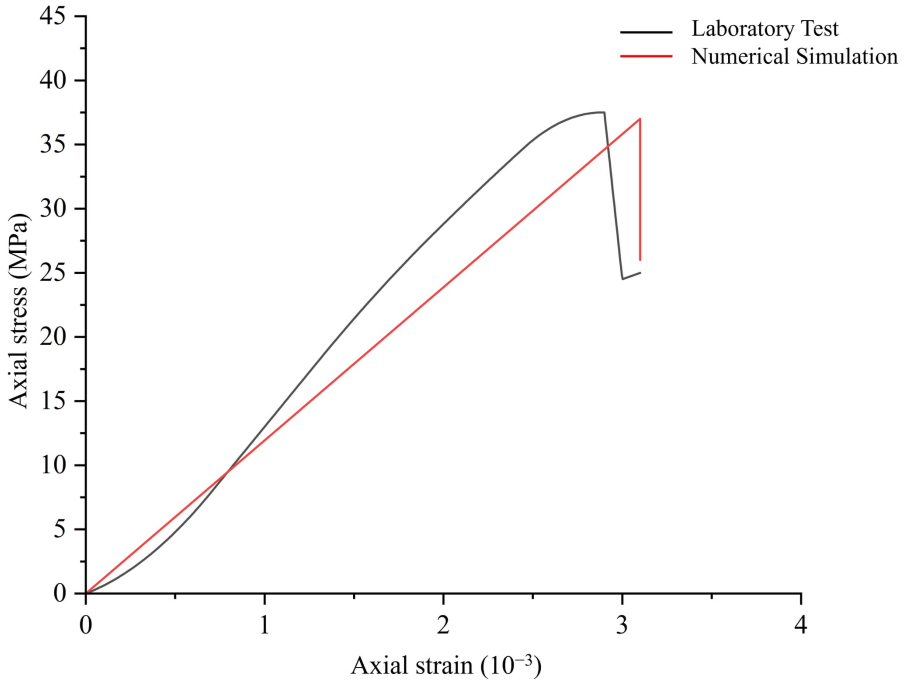


Figure 5. Comparison of laboratory and DDA numerical results for fine-grained sandstone under uniaxial compression.

The uniaxial compression test results provided experimental support for calibrating the microscopic parameters of the different strata. The numerical model of the 1210 panel developed using these parameters was primarily used to compare overburden and surface responses under the specified simulation conditions. The panel-scale model remains to be validated against subsequent field monitoring data.

As shown in Figure 6, a numerical model of partial backfill mining is constructed using NPR-DDA, with a horizontal length of 1200 m and a vertical height of 700 m. The model contains 218,047 computational particles, with a specified minimum particle size of 0.5 m and a maximum-to-minimum particle size ratio of 1.6. Horizontal displacement is restrained at both lateral boundaries, while vertical displacement is permitted. Both horizontal and vertical displacements are restrained at the bottom boundary, and the top boundary is free. Self-weight stress is generated by applying a gravitational acceleration of 9.8 m/s^2. Mining starts from a cut located 150 m from the left boundary and proceeds in increments of 50 m for ten successive stages, giving a cumulative advance of 500 m. The backfill rate, backfill working face width, caving working face width, and section coal pillar width are specified according to the corresponding parametric simulation schemes. The material input parameters are listed in Table 1.

In the NPR-DDA simulations, the velocity attenuation index of the bonded elements was set to 5000, the computational time step was set to 1×10^{-5} s, and the convergence tolerance was set to 1×10^{-8}.

As the model size increases, the growing numbers of blocks and contacts increase the computational cost of NPR-DDA. GPU/CUDA parallel computing offers a potential approach to improving the efficiency of large-scale discontinuum simulations. For example, Liu and Wong implemented CUDA parallelization of modules including contact detection and contact force calculation in their FDM/FDEM thermomechanical coupling model, providing a reference for improving the efficiency of related numerical methods [23]. Their approach may inform future parallelization of the NPR-DDA code.

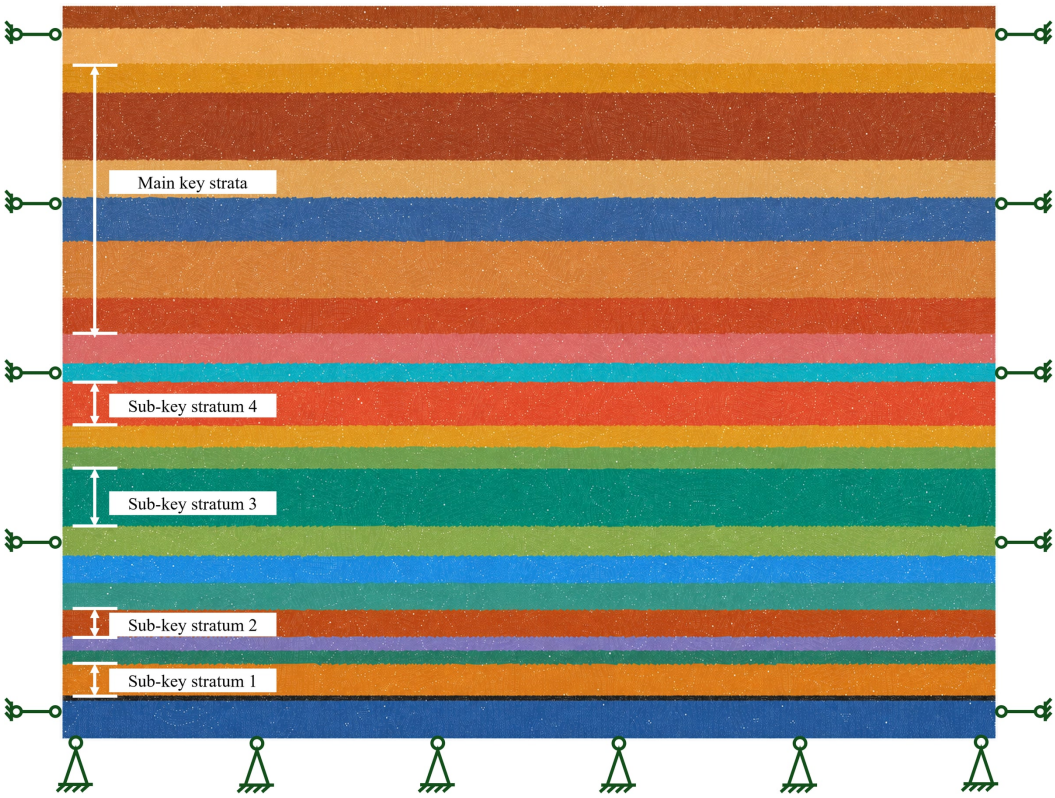


Figure 6. Numerical calculation model.

Table 1. Microscopic parameters of the numerical model for the 1210 panel.

Rock Stratum Name	Unit Weight/kN·m^{-3}	Elastic Modulus/GPa	Cohesion/MPa	Internal Friction Angle/°	Poisson's Ratio	Tensile Strength/MPa
Topsoil	23	1.1	3.0	30.0	0.3	0.2
Fine-grained sandstone	24	8.4	3.0	35.0	0.3	1.4
Fine-grained sandstone	21	2.2	4.0	45.0	0.23	1.1
Medium-grained sandstone	23	4.1	4.0	43.0	0.3	0.6
Fine-grained sandstone	23	7.2	5.0	45.0	0.3	0.6
Siltstone	21	5.0	4.0	40.0	0.3	0.6
Fine-grained sandstone	21	5.2	4.0	45.0	0.3	0.7
Medium-grained sandstone	21	8.5	4.0	45.6	0.3	0.8
Medium-grained sandstone	21	7.2	9.0	45.0	0.3	1.1
Siltstone	22	9.9	5.0	45.0	0.23	1.5
Medium-grained sandstone	23	11.6	4.5	46.9	0.3	2.2
Fine-grained sandstone	24	13.6	10.0	50.0	0.23	5.7
Sandy mudstone	24	14.4	15.0	40.0	0.23	4.3
Sandy mudstone	22	15.5	15.0	30.0	0.23	3.3
Fine-grained sandstone	24	14.4	10.0	30.0	0.3	2.2
Siltstone	23	13.1	15.0	35.0	0.23	1.3
Sandy mudstone	22	19.0	15.0	40.0	0.23	1.2
Medium-grained sandstone	23	11.4	5.0	40.0	0.23	1.5
Siltstone	23	4.1	4.0	35.0	0.23	1.7
Sandy mudstone	22	19.0	15.0	35.0	0.23	1.9
Fine-grained sandstone	24	14.4	6.0	35.0	0.23	1.7
2-2 upper coal seam	18	3.3	1.5	30.0	0.3	1.5
Siltstone	23	10.1	20.0	35.0	0.23	1.8

3.2. Vertical Displacement and Stress Distribution Characteristics of Partial Backfill Mining

The shear strength of the bonds between backfill particles is determined using the Mohr–Coulomb criterion. Shear failure occurs when the shear stress at a bond exceeds its shear strength, whereas tensile failure occurs when the tensile stress exceeds its tensile strength. The backfill zone is assigned coal gangue backfill material parameters based on the parameter values documented in the associated study [24]. As shown in Table 2, the

bulk modulus is 0.21 GPa, the shear modulus is 0.095 GPa, the density is 1500 kg/m^3, the Poisson's ratio is 0.30, the cohesion is 2 MPa, the friction angle is 28°, and the tensile strength is 1.5 MPa.

Table 2. Material parameters of the coal gangue backfill zone.

Bulk Modulus/GPa	Shear Modulus/GPa	Friction Angle/°	Cohesion/MPa	Density/(kg/m^3)	Poisson's Ratio	Tensile Strength/MPa
0.21	0.095	28	2	1500	0.3	1.5

As shown in Figure 7, which presents the vertical displacement distribution contour map of partial backfill mining, it can be seen that above the caving mining working faces on both sides, significant V-shaped subsidence funnel structures are induced. The displacement contour lines in this area are highly dense, and the blue extreme-value zones representing high subsidence have a wide distribution range and a large downward penetration depth. In sharp contrast to the caving zones on both sides, the displacement response above the central backfill working face is buffered and restricted. The color distribution of this area in the contour map is obviously lighter, and both the extent and subsidence depth of the deep blue zones representing deep failure have been significantly suppressed and reduced. The displacement contrast between the strata above the central backfill zone and those above the caving zones on both sides reflects the spatially nonuniform overburden deformation under the partial backfill arrangement. The smaller subsidence in the central region is consistent with the support provided by the backfill zone, suggesting that partial backfilling helps limit the downward movement of the overlying strata.

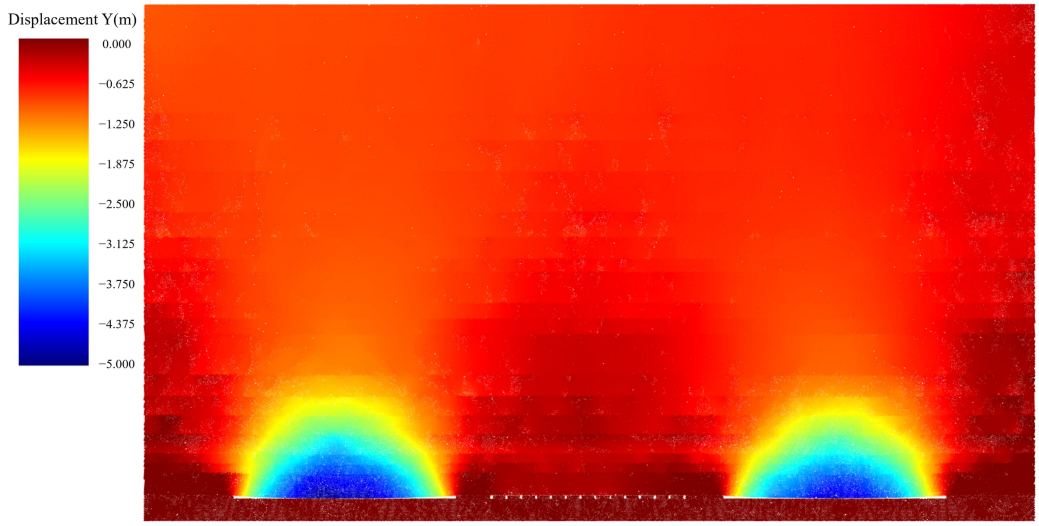


Figure 7. Vertical displacement distribution contour map of partial backfill mining.

Figure 8 presents the vertical stress distribution along a monitoring line located 2 m above the coal seam under partial backfill mining. The segments corresponding to the caving zones on both sides generally exhibit lower stresses, indicating mining-induced stress relief. The segment corresponding to the central backfill zone exhibits higher stresses, with a mean vertical stress of 19.38 MPa, and local stress peaks occur near the regional boundaries. This distribution reflects stress redistribution in the strata above the different mining regions. Together with the smaller subsidence in the central region shown in Figure 7, these results demonstrate distinct deformation and stress responses between the central region and the caving regions on both sides under the partial backfill arrangement.

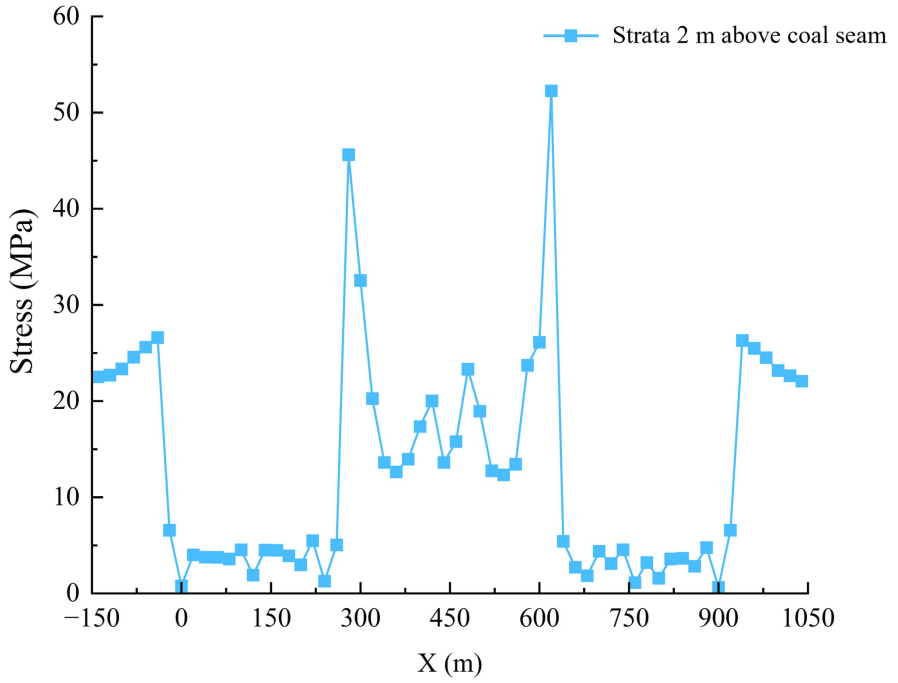


Figure 8. Vertical stress distribution graph of partial backfill mining.

4. Analysis of Surface Subsidence Control in Partial Backfill Mining

4.1. Influence of Backfill Rate

In the field of backfill technology, the regulation of strata movement and energy accumulation is restricted by many factors, and its core issue is reflected in the variation law of the effective subsidence space of the roof. In this two-dimensional model, the backfill rate represents the target backfill height as a proportion of the corresponding goaf height. Numerically, the target backfill height is determined by multiplying the goaf height by the prescribed backfill rate. Backfill particles are generated within this height range, and the associated bonding parameters are specified using the calibrated backfill material properties. Four backfill rates of 60%, 70%, 80%, and 90% are considered, corresponding to backfill heights of 60%, 70%, 80%, and 90% of the goaf height, respectively. The remaining parameters are held constant, as summarized in Table 3.

Table 3. Research scheme on the influence of different backfill rates on surface subsidence.

Isolation Coal Pillar/m	Caving Working Face Width/m	Backfill Working Face Width/m	Backfill Rate
30	300	300	90%
			80%
			70%
			60%

Based on the design schemes provided in Table 3, an in-depth analysis was conducted utilizing the NPR-DDA numerical simulation software, and key data on surface subsidence were systematically acquired. On this basis, vertical displacement contour maps and surface subsidence curves were plotted (see Figures 9 and 10).

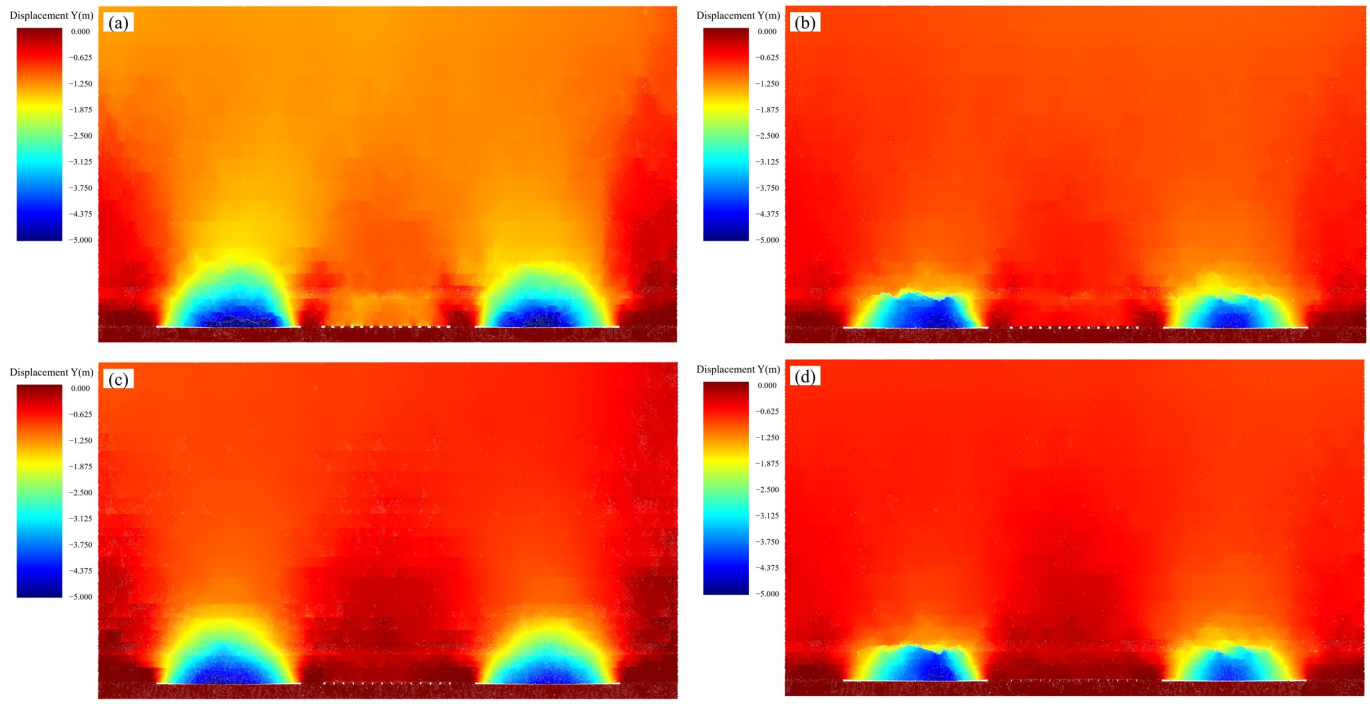


Figure 9. Vertical displacement contour maps of partial backfill mining under different backfill rates. (**a**) Backfill rate of 60%; (**b**) Backfill rate of 70%; (**c**) Backfill rate of 80%; (**d**) Backfill rate of 90%.

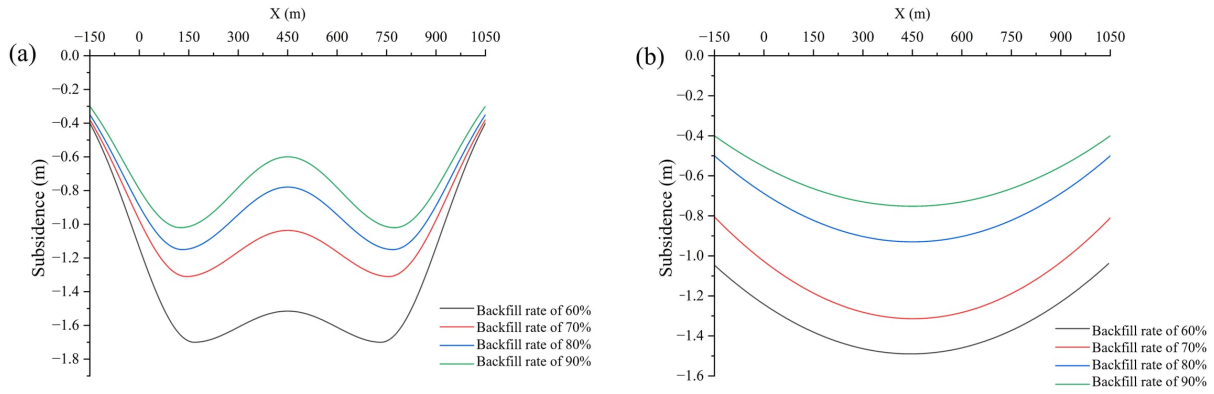


Figure 10. Strata subsidence curves of partial backfill mining under different backfill rates. (**a**) 260 m above the coal seam; (**b**) Surface.

To illustrate the impact of backfill rate variations on the surface subsidence control effect in the partial backfill mining area, the maximum surface subsidence data under different backfill rate conditions were selected to plot the corresponding relationship curve, as shown in Figure 11.

Within the investigated backfill rate range of 60–90%, the magnitude of maximum surface subsidence decreases as the backfill rate increases. A linear function is used to empirically fit the simulation results in this group and describe the trend under the corresponding simulation conditions, as expressed in Equation (1). Here, x denotes the backfill rate expressed as a decimal, and W_{max} denotes the signed displacement at the location of maximum subsidence magnitude, with negative values indicating downward displacement. The slope describes the fitted displacement change per unit change in backfill rate, while the intercept determines the position of the fitted line.

$$W_{max} = 2733x - 3099 \quad (1)$$

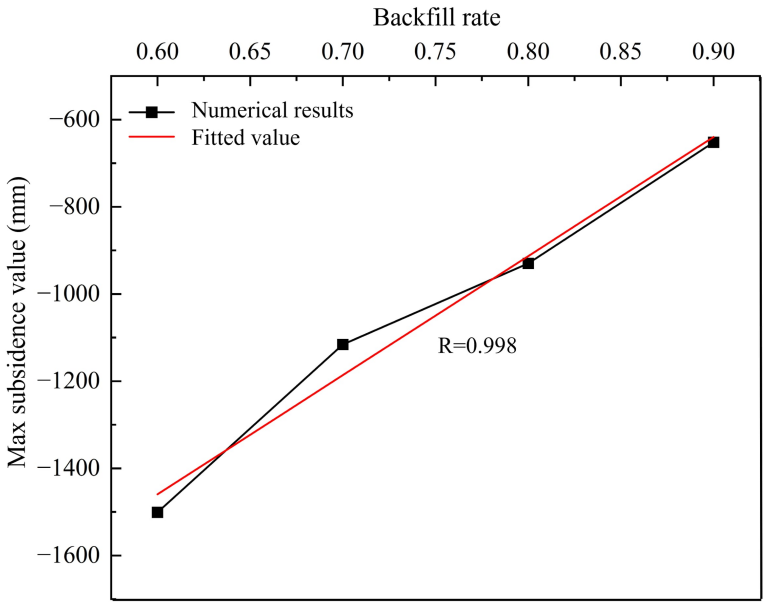


Figure 11. Relationship between the backfill rate and the maximum subsidence value.

According to the analysis of the statistical data in Table 4, as the backfill rate gradually increases from 60% to 90%, the maximum surface subsidence decreases from −1501 mm to −652 mm, with an absolute subsidence reduction reaching 849 mm. This variation in data indicates that the backfill rate plays a key role in regulating the evolution of surface deformation. In this model, the backfill rate is varied by changing the target backfill height, while the initial porosity, material input parameters, and bonding parameters remain unchanged. Increasing the target backfill height reduces the unfilled space available for downward movement of the overlying strata, providing a geometric explanation for the reduction in surface subsidence. This mechanism of replacing the mined-out space through active support is mechanically similar to the control law of reducing the actual mining height on surface subsidence, ultimately presenting a more significant suppression effect on surface subsidence.

Table 4. Statistics of surface subsidence extreme values under different backfill rates.

Fixed Parameters	Backfill Rate	Maximum Subsidence Value/mm
Caving working face width 300 m Backfill working face width 300 m Section coal pillar width 30 m	60%	−1501
	70%	−1316
	80%	−930
	90%	−652

4.2. Influence of Mining, Backfilling, and Retaining Dimensions

4.2.1. Influence of Backfill Working-Face Width

Table 5 presents the research scheme on the influence of different backfill working-face widths on surface subsidence. Based on this design scheme, the research is conducted using the NPR-DDA numerical simulation software. First, the surface subsidence data are extracted to obtain the vertical displacement distribution contour maps and surface subsidence variation curves, as specifically shown in Figures 12 and 13.

Table 5. Research scheme on the influence of backfill working-face width on surface subsidence.

Isolation Coal Pillar/m	Caving Working Face Width/m	Backfill Working Face Width/m	Backfill Rate
30	300	150	80%
		200	
		250	
		300	

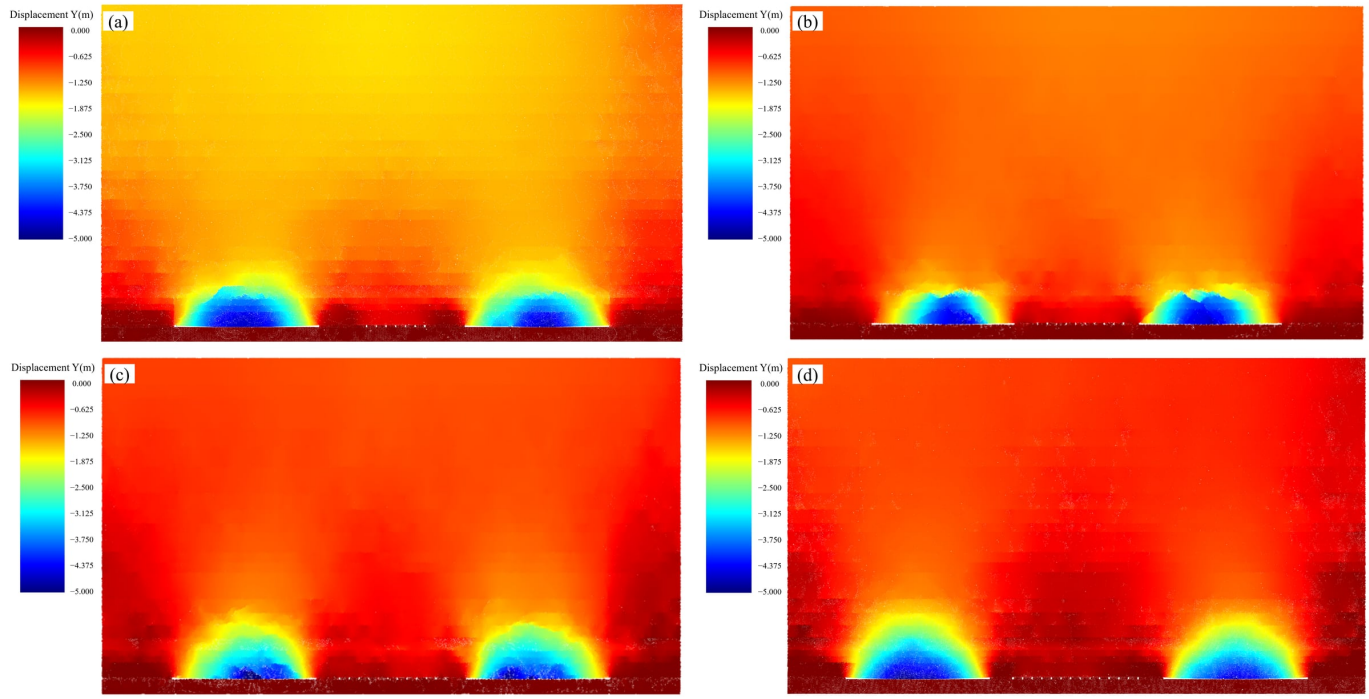


Figure 12. Vertical displacement contour maps of partial backfill mining under different backfill working-face widths. (**a**) Backfill working face width 150 m; (**b**) Backfill working face width 200 m; (**c**) Backfill working face width 250 m; (**d**) Backfill working face width 300 m.

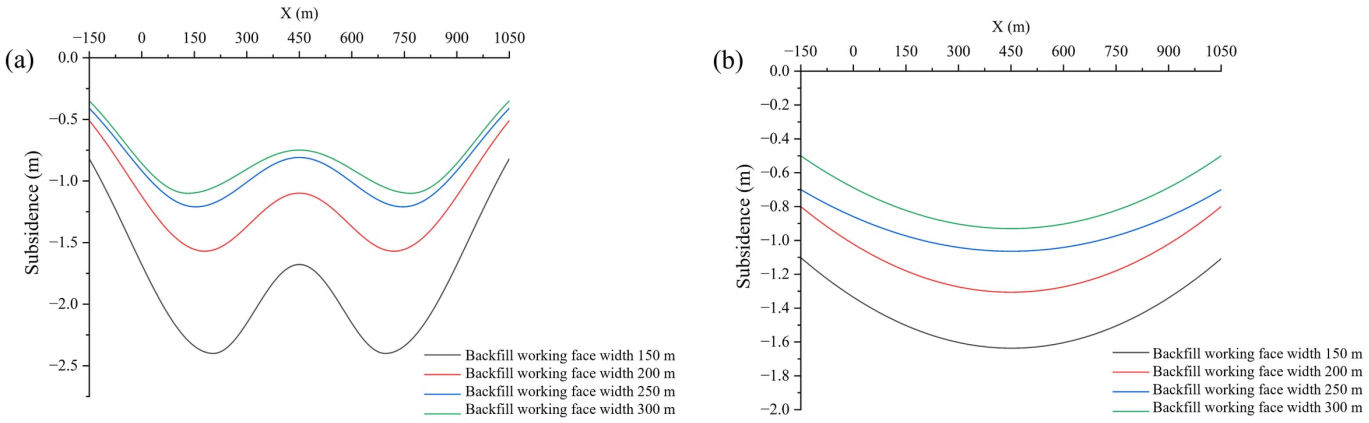


Figure 13. Strata subsidence curves of partial backfill mining under different backfill working-face widths. (**a**) 260 m above the coal seam; (**b**) Surface.

To better present the relevant influences, this paper selects specific backfill mining scenarios for research and calculates the distribution.

Figure 14 shows that the magnitude of maximum surface subsidence decreases as the backfill working face width increases within the investigated range of 150–300 m, with progressively smaller reductions. A logarithmic function is used to empirically fit the simulation results in this group and describe this trend, as expressed in Equation (2). Here, x denotes the numerical value of the backfill working face width expressed in meters, and the fitted coefficients jointly determine the position and rate of change of the curve.

$$W_{\max} = -4169 + 604\,ln(x - 83) \quad (2)$$

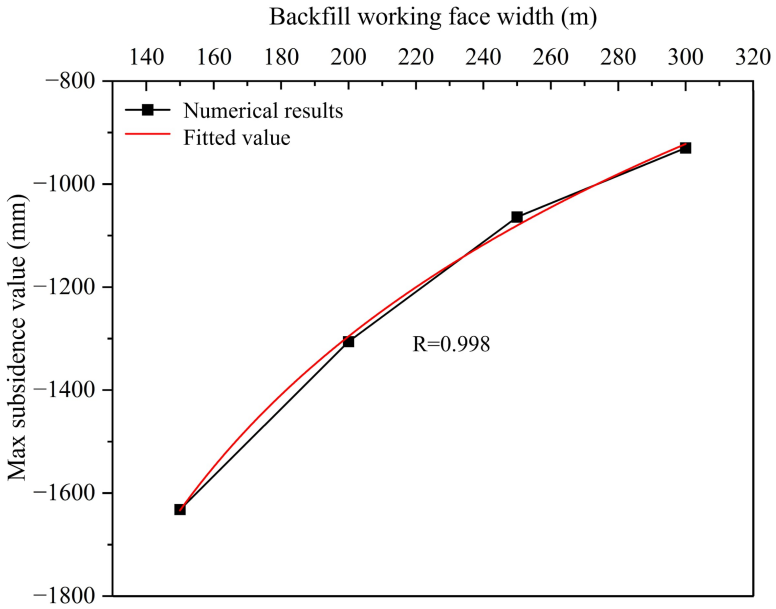


Figure 14. Relationship between the backfill working-face width and the subsidence value.

Table 6 shows the statistics of surface subsidence extreme values under different backfill working-face widths. It can be seen that when the backfill working-face width expands from 150 m to 300 m, the maximum surface subsidence non-linearly decreases from −1632 mm to −930 mm, with the absolute subsidence reduction reaching 702 mm. Analyzing from the perspective of the overburden movement mechanism, the increase in the backfill working-face width essentially enlarges the physical span between the adjacent caved goafs on both sides, effectively weakening the interference of the mining-induced stress and displacement fields above the two independent caving zones, and prompting the global overburden failure to exhibit a regional distribution characteristic of partially independent and discontinuous mining. Controlled by the discontinuous evolution law, the overall surface subsidence movement trend gradually flattens out. Under the conditions adopted in this simulation group, increasing the backfill working face width reduces the magnitude of maximum surface subsidence and affects the spatial distributions of mining-induced displacement and stress.

Table 6. Statistics of surface subsidence extreme values under different backfill working-face widths.

Fixed Parameters	Backfill Working Face Width/m	Maximum Subsidence Value/mm
Caving working face width 300 m Backfill rate 80% Section coal pillar width 30 m	150	−1632
	200	−1306
	250	−1064
	300	−930

4.2.2. Influence of Caving Working-Face Width

Based on the scheme designed in Table 7, the research is conducted using the NPR-DDA numerical simulation software. According to the obtained surface subsidence data, the vertical displacement distribution contour maps and surface subsidence variation curves are obtained, as shown in Figures 15 and 16.

Table 7. Research scheme on the influence of caving working-face width on surface subsidence.

Isolation Coal Pillar/m	Caving Working Face Width/m	Backfill Working Face Width/m	Backfill Rate
30	200	150	80%
	250		
	300		
	350		

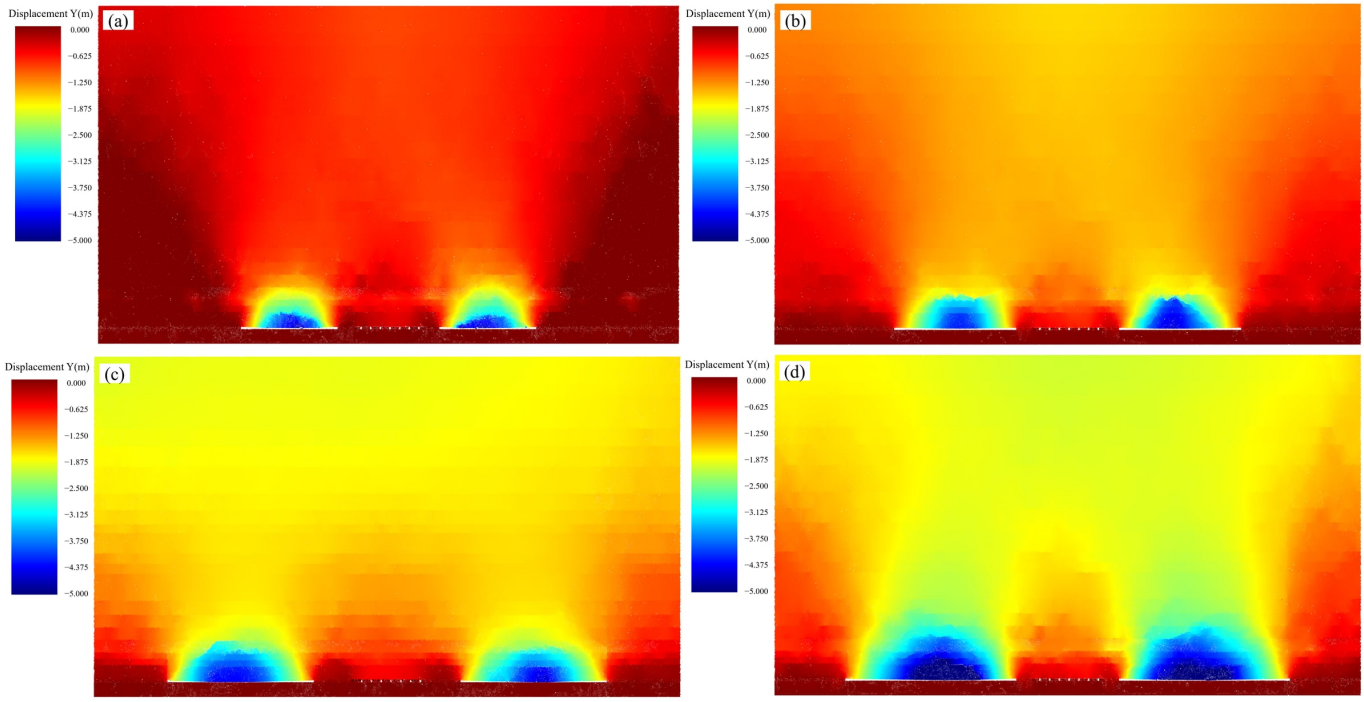


Figure 15. Vertical displacement contour maps of partial backfill mining under different caving working-face widths. (**a**) Caving working face 200 m; (**b**) Caving working face 250 m; (**c**) Caving working face 300 m; (**d**) Caving working face 350 m.

To present the impact of variations in the caving working-face width on the surface subsidence control of backfill mining, the corresponding relationship between different caving working-face widths and the maximum surface subsidence is calculated, as shown below (see Figure 17 and Table 8 for details).

Figure 17 shows that the magnitude of maximum surface subsidence increases as the caving working-face width increases within the investigated range of 200–350 m. A quadratic function is used to empirically fit the simulation results in this group and describe the nonlinear trend under the corresponding simulation conditions, as expressed in Equation (3). Here, x denotes the numerical value of the caving working face width expressed in meters. The linear and quadratic coefficients jointly describe the rate of change and

curvature of the fitted response, while the constant term determines the vertical position of the curve.

$$W_{max} = 15.38x - 0.04x^2 - 2371.4 \quad (3)$$

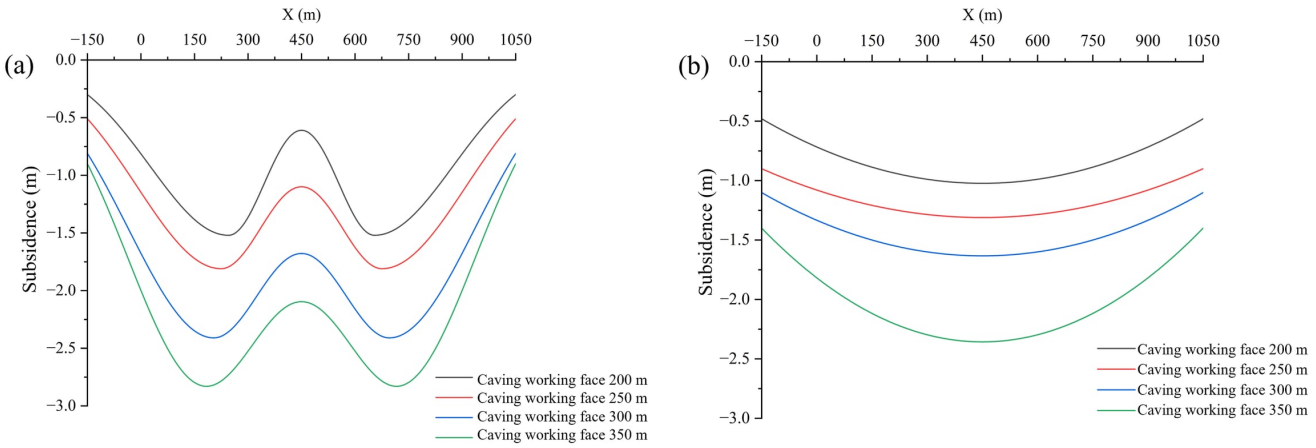


Figure 16. Strata subsidence curves of partial backfill mining under different caving working-face widths. (**a**) 260 m above the coal seam; (**b**) Surface.

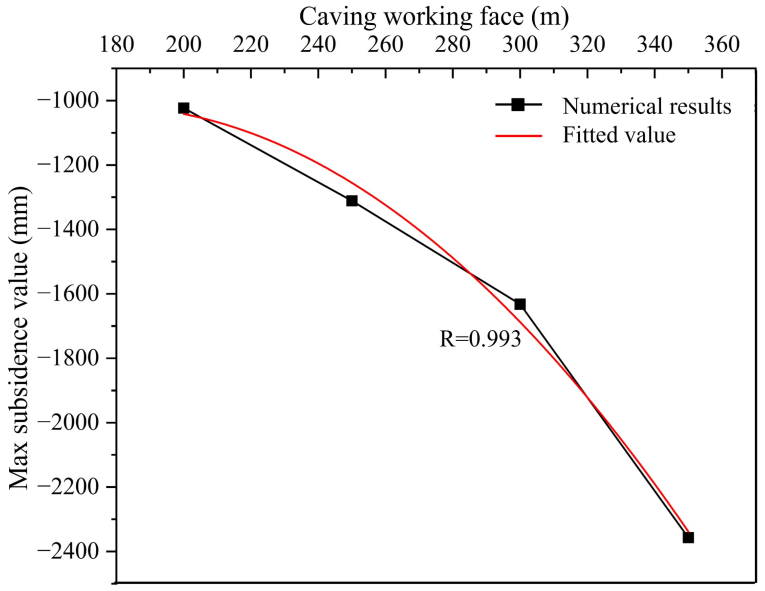


Figure 17. Relationship between the caving working-face width and the subsidence value.

Table 8. Statistics of surface subsidence extreme values under different caving working-face widths.

Fixed Parameters	Caving Working Face Width/m	Maximum Subsidence Value/mm
Backfill working face width 150 m Backfill rate 80% Section coal pillar width 30 m	200	−1023
	250	−1311
	300	−1632
	350	−2357

As can be seen from Table 8, the increase in the width of the caving working face has a significant nonlinear expansion effect on surface subsidence. When the width of the caving

working face increases from 200 m to 350 m, the maximum surface subsidence increases from −1023 mm to −2357 mm, with an absolute subsidence increment reaching 1334 mm. The expansion of the transverse scale of the caving working face directly leads to a significant increase in the geometric volume of the underlying goaf, weakens the bearing capacity of the overlying strata, and prompts the scope of overburden failure and the depth of influence to rapidly expand towards the high-level rock series, thereby inducing a large-scale regional systemic caving. The variation in the width of the caving working face is one of the main influencing factors, and its impact on surface subsidence is particularly obvious.

4.2.3. Influence of Section Coal-Pillar Width

Based on the design parameters given in Table 9, the research is conducted using the NPR-DDA numerical simulation software. The software is used to extract the surface subsidence data, obtaining the vertical displacement distribution contour maps and surface subsidence curves. The specific results are shown in Figures 18 and 19:

Table 9. Research scheme on the influence of section coal-pillar width on surface subsidence.

Isolation Coal Pillar/m	Caving Working Face Width/m	Backfill Working Face Width/m	BACKFILL RATE
25	300	300	80%
30			
50			
60			

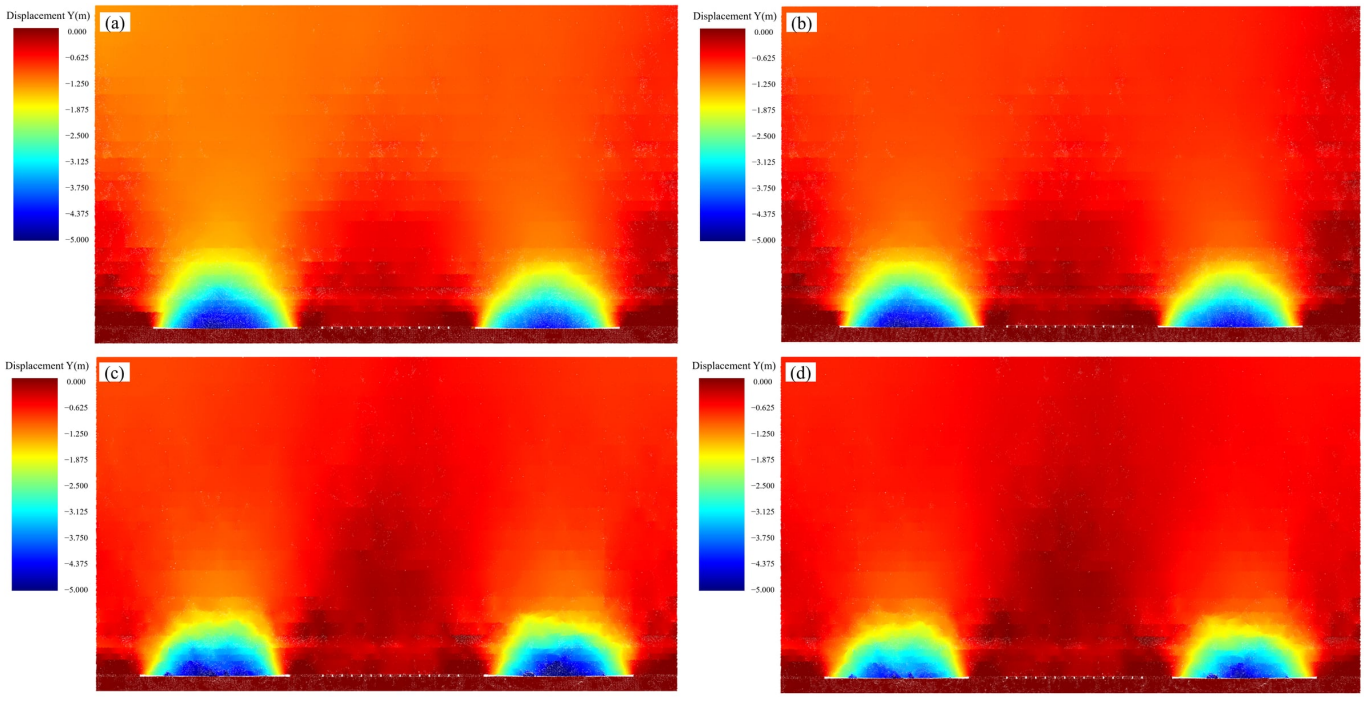


Figure 18. Vertical displacement contour maps of partial backfill mining under different section coal-pillar widths. (**a**) Isolation coal pillar 25 m; (**b**) Isolation coal pillar 30 m; (**c**) Isolation coal pillar 50 m; (**d**) Isolation coal pillar 60 m.

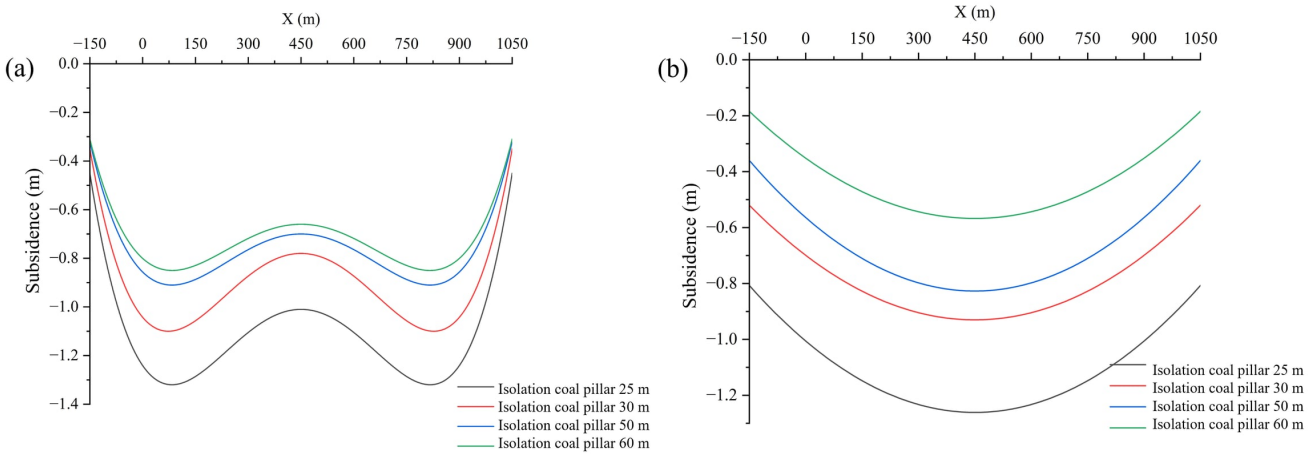


Figure 19. Strata subsidence curves of partial backfill mining under different section coal-pillar widths. (**a**) 260 m above the coal seam; (**b**) Surface.

To intuitively observe the impact of variations in the section coal-pillar width on the surface subsidence control effect of partial backfill mining, the maximum surface subsidence values corresponding to each section coal-pillar width were calculated.

Figure 20 shows that the magnitude of maximum surface subsidence decreases as the section coal-pillar width increases within the investigated range of 25–60 m. A linear function is used to empirically fit the simulation results in this group and describe the overall trend under the corresponding simulation conditions, as expressed in Equation (4). Here, x denotes the numerical value of the section coal pillar width expressed in meters. The slope describes the fitted displacement change associated with a 1 m increase in coal pillar width, while the intercept determines the position of the fitted line.

$$W_{\max} = 14.47x - 1543.79 \quad (4)$$

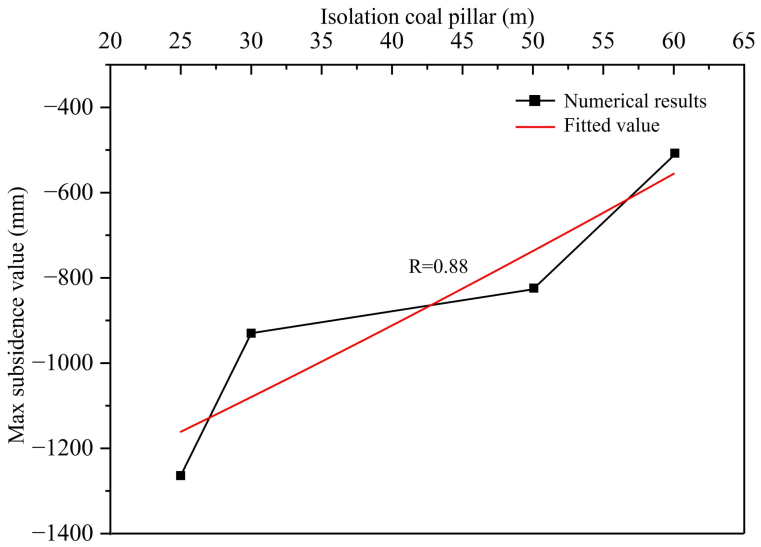


Figure 20. Relationship between the section coal-pillar width and the subsidence value.

Table 10 shows the statistical data of surface subsidence extreme values under different section coal-pillar widths. It can be found that when the section coal-pillar width expands from 25 m to 60 m, the maximum surface subsidence value decreases from −1264 mm to −513 mm, with an absolute subsidence reduction of 751 mm. Increasing the coal pillar width enlarges the retained support region, consistent with the reduction in surface subsidence

observed in this simulation group. Under the conditions adopted in this simulation group, increasing the section coal pillar width from 25 m to 60 m reduces the magnitude of maximum surface subsidence by 751 mm, indicating a substantial effect on subsidence control in the simulated cases.

Table 10. Statistics of surface subsidence extreme values under different section coal-pillar widths.

Fixed Parameters	Section Coal Pillar Width/m	Maximum Subsidence Value/mm
Backfill working-face width 300 m Caving working-face width 300 m Backfill rate 80%	25	−1264
	30	−930
	50	−827
	60	−513

4.3. Discussion

The simulation results under the investigated conditions show that increasing the backfill rate, backfill working face width, or section coal pillar width helps reduce surface subsidence, whereas increasing the caving working face width aggravates surface subsidence. Variations in the backfill rate and backfill working face width reflect the effects of backfilling conditions on subsidence control, while variations in the caving working face width and section coal pillar width reflect the effects of the layout of mined areas and retained coal pillars. These results provide a reference for examining surface responses under different parameter configurations.

This study adopts a one-factor-at-a-time approach, varying the target parameter while holding the remaining parameters constant within each simulation group. The backfill working face width is fixed at 150 m in the caving working face width group and at 300 m in the other three groups. Accordingly, the results of each group correspond to its specific parameter configuration. Based on the geological conditions of the 1210 panel, the analysis focuses on the individual effects of the factors and aims to provide a reference for developing practical mining schemes. Numerical convergence through particle-size and model-boundary sensitivity analyses has not been assessed in this study.

5. Conclusions

(1) Field measurements from the completed 1208 panel show that mining-induced surface subsidence exhibits a progressively developing, asymmetric, funnel-shaped distribution. After crossing the geometric inflection point, the subsidence rate accelerates significantly, with the maximum subsidence point (187 mm) located at monitoring point H52, which is shifted to the left relative to the geometric center of the goaf.

(2) Under the simulated partial backfill mining conditions, pronounced subsidence concentrations develop above the caving zones on both sides, whereas subsidence above the central backfill zone is relatively smaller. The monitoring line located 2 m above the coal seam shows lower stresses in the segments corresponding to the caving zones, higher stresses in the segment corresponding to the central backfill zone, and local stress concentrations near the regional boundaries. The mean vertical stress in the segment corresponding to the central backfill zone is 19.38 MPa. These results reveal spatial differences in overburden displacement and stress distributions under the partial backfill arrangement.

(3) Under the geological conditions of the 1210 panel at the Shilawusu Coal Mine and the fixed parameter settings of the respective simulation groups, increasing the backfill rate from 60% to 90%, the backfill working face width from 150 m to 300 m, and

the section coal pillar width from 25 m to 60 m reduces the magnitude of maximum surface subsidence by 849 mm, 702 mm, and 751 mm, respectively. Increasing the caving working face width from 200 m to 350 m increases the magnitude of maximum surface subsidence by 1334 mm. These results represent the effects of individual factors under the corresponding simulation conditions.

Author Contributions: Methodology, C.W.; software, C.W.; validation, C.W., W.G. and Y.G.; formal analysis, C.W. and C.H.; resources, C.W.; data curation, Y.G.; writing—original draft preparation, C.W.; writing—review and editing, C.W. and Q.Z.; visualization, W.G.; project administration, C.H.; funding acquisition, Q.Z. All authors have read and agreed to the published version of the manuscript.

Funding: This research was funded by the National Natural Science Foundation of China, grant number 42602340, and the Hubei Provincial Natural Science Foundation of China, grant number 2026AFB004.

Data Availability Statement: The data presented in this study are available on request from the corresponding author. The data are not publicly available due to privacy.

Conflicts of Interest: Authors Chao Wang and Weiming Gao were employed by the company Yankuang Energy Group. Author Yingshi Gu was employed by the company Inner Mongolia Haosheng Coal Industry. The remaining authors declare that the research was conducted in the absence of any commercial or financial relationships that could be construed as potential conflicts of interest.

References

1. Guo, G.L.; Zha, J.F. *Mining Subsidence Science*; China University of Mining and Technology Press: Xuzhou, China, 2020; ISBN 978-7-5646-1174-3.
2. Chen, S.J.; Yin, D.W.; Cao, F.W.; Liu, Y.; Ren, K.Q. An overview of integrated surface subsidence-reducing technology in mining areas of China. *Nat. Hazards* **2016**, *81*, 1129–1145. [CrossRef]
3. Xie, H.P.; Duan, F.B.; Zhou, H.W.; Zhao, G.X. Recent development of theory and application of backfilling mining technology in China's coal mining areas. *China Min. Mag.* **1998**, *7*, 37–41.
4. Liu, J.G.; Li, X.W.; He, T. Application status and prospect of backfill mining in Chinese coal mines. *J. China Coal Soc.* **2020**, *45*, 141–150. [CrossRef]
5. Hu, B.N.; Liu, P.L.; Cui, F.; Wang, H.Y. Review and development status of backfill coal mining technology in China. *Coal Sci. Technol.* **2020**, *48*, 39–47. [CrossRef]
6. Zhang, Q.; Zhang, J.X.; Wu, Z.Y.; Chen, Y. Overview of solid backfilling technology based on coal-waste underground separation in China. *Sustainability* **2019**, *11*, 2118. [CrossRef]
7. Chang, Q.L.; Zhou, H.Q.; Bai, J.B.; Duan, C.R.; Li, Y.W. Stability study and practice of overlying strata with paste backfilling. *J. Min. Saf. Eng.* **2011**, *28*, 279–282. [CrossRef]
8. Sun, K.; Zhang, J.X.; He, M.C.; Li, M.; Guo, S.J. Control of surface deformation in mining areas by underground backfilling with solid waste from coal preparation: A case study. *Sci. Total Environ.* **2023**, *891*, 164693. [CrossRef] [PubMed]
9. Meng, Z.X.; Dong, Y.; Zhang, X.G.; Jiao, F.S.; Fan, Y.Q.; Thammavongsa, C. Short-wall paste continuous mining and continuous backfilling technology for controlling surface subsidence. *Front. Earth Sci.* **2023**, *10*, 1009617. [CrossRef]
10. Xuan, D.Y.; Xu, J.L. Grout injection into bed separation to control surface subsidence during longwall mining under villages: Case study of Liudian coal mine, China. *Nat. Hazards* **2014**, *73*, 883–906. [CrossRef]
11. Yang, K.; Feng, X.W.; He, X.; Han, L.; Ma, G.J.; Zhao, X.Y.; Zhang, J.Q.; Yu, X.; Liu, Z. Spatial dynamic evolution law of overlying strata fracture field under continuous mining and filling. *Coal Sci. Technol.* **2026**, *54*, 84–99. [CrossRef]
12. Ma, Q. Research on High-Efficiency Paste Layered Backfill Mining Technology and Overburden Movement Law. Doctoral Dissertation, China University of Mining and Technology, Xuzhou, China, 2023.
13. Zhang, M. Theoretical Research on Overburden Control in High-Efficiency Paste Backfill Working Face. Doctoral Dissertation, China University of Mining and Technology, Xuzhou, China, 2019. [CrossRef]
14. Li, S.L.; Feng, T.; Zhu, Z.H. Mechanical model of rock beam with both ends fixed and force analysis of roof fracture in cemented filling mining. *J. Cent. South Univ. Sci. Technol.* **2014**, *45*, 2793–2798.
15. Zhou, Y.B. Study on Continuous Movement and Deformation Law of Overburden and Subsidence Prediction in Backfill Mining. Doctoral Dissertation, China University of Mining and Technology (Beijing), Beijing, China, 2021. [CrossRef]

16. Guo, M.J.; Guo, W.B.; Tan, Y.; Zhang, H.B.; Zheng, Q.L.; Zhao, G.B.; Bai, E. Ground control by L-shaped ground fracture patterns for spatial characteristics of overlying strata under mining disturbance. *Geomech. Geophys. Geo-Energy Geo-Resour.* **2024**, *10*, 31. [CrossRef]
17. Hao, J.; Chen, A.F.; Li, X.L.; Bian, H.; Shi, Y.K.; Wang, X.; Zhao, J.L.; Liu, H.J. A case study of pillar extraction under weak thick mudstone roof stratum: Mining scheme design and strata control. *Front. Earth Sci.* **2022**, *10*, 1051245. [CrossRef]
18. Zhu, X.; Zha, F.; Guo, G.L.; Zhang, P.F.; Cheng, H.; Liu, H.; Yang, X.Y. Subsidence Control Design Method and Application to Backfill-Strip Mining Technology. *Adv. Civ. Eng.* **2021**, *2021*, 5177174. [CrossRef]
19. Wang, F.; Jiang, B.Y.; Chen, S.J.; Ren, M.Z. Surface collapse control under thick unconsolidated layers by backfilling strip mining in coal mines. *Int. J. Rock Mech. Min. Sci.* **2019**, *113*, 268–277. [CrossRef]
20. Du, Z.W.; Chen, D.Y.; Li, X.L.; Jian, Y.; Zhang, W.Z.; Zhang, D.D.; Tian, Y.F. Study on partial paste backfilling in a longwall panel based on the background of thick unconsolidated layers and thin bedrock. *Sustainability* **2024**, *16*, 4393. [CrossRef]
21. Liu, J.W.; Sui, W.H.; Zhao, Q.J. Environmentally sustainable mining: A case study of intermittent cut-and-fill mining under sand aquifers. *Environ. Earth Sci.* **2017**, *76*, 562. [CrossRef]
22. Huang, G.H.; Dai, J.L.; Zhang, S.; Yi, X.W.; Tong, C.X. A new bonded-particle model for simulation of rock failure and its application in roadway stability analysis. *Comput. Geotech.* **2025**, *183*, 107182. [CrossRef]
23. Liu, Z.; Wong, L.N.Y. On the GPGPU-accelerated thermomechanical coupling finite-difference method/hybrid finite-discrete element method (FDM/FDEM) model for geomaterials. *Eng. Geol.* **2025**, *358*, 108383. [CrossRef]
24. Guo, G.L.; Zhu, X.J.; Zha, J.F.; Wang, Q. Subsidence prediction method based on equivalent mining height theory for solid backfilling mining. *Trans. Nonferrous Met. Soc. China* **2014**, *24*, 3302–3308. [CrossRef]

Disclaimer/Publisher's Note: The statements, opinions and data contained in all publications are solely those of the individual author(s) and contributor(s) and not of MDPI and/or the editor(s). MDPI and/or the editor(s) disclaim responsibility for any injury to people or property resulting from any ideas, methods, instructions or products referred to in the content.